Fermi National Accelerator Laboratory

FN-386
1500.000

CHAOS, BEAM BLOW-UP AND RESONANCE OVERLAP IN THE BEAM-BEAM INTERACTION

D. Neuffer

May 1983

Operated by Universities Research Association Inc. under contract with the United States Department of Energy

CHAOS, BEAM BLOW-UP AND RESONANCE OVERLAP IN THE BEAM-BEAM INTERACTION

David Neuffer
Fermi National Accelerator Laboratory
P.O. Box 500
Batavia, Illinois 60510

Abstract

Simulations of the beam-beam interaction have shown chaotic motion in 2-D simulations and have shown beam blow-up with chaotic motion in simulations with tune modulation. [1-13] A simple resonance model is developed to analyze these results. The density of chaotic motion in the former cases are accurately estimated by the calculated resonance overlap area of low order resonances. In the latter cases, "beam blowup" is found to occur when the modulation subresonances of a low order resonance intersect. Other simulation features are compared with the resonant model. We conclude that this resonance model with application of resonance overlap conditions similar to the "Chirikov" criterion [14] is useful in predicting beam response in the multidimensional beam-beam interaction with tune modulation.

IA. Summary of Simulation Results

In previous notes and papers [1-13], we have presented results of simulations of the beam-beam interaction. Some features of these simulations are summarized in this section.

The basic procedure in these simulations was the propagation of a set of particle trajectories through many turns of the collider. Transport around one turn is simulated as the product of two matrix multiplications in both (x and y) transverse dimensions:

$$\begin{pmatrix} x \\ x' \end{pmatrix}_{after} = \begin{pmatrix} \cos(2\pi\nu_x) & \beta_0 \sin(2\pi\nu_x) \\ \frac{-1}{\beta_0}\sin(2\pi\nu_x) & \cos(2\pi\nu_x) \end{pmatrix} \begin{pmatrix} 1 & 0 \\ \frac{-4\pi\Delta\nu}{\beta_0} F(x,y) & 1 \end{pmatrix} \begin{pmatrix} x \\ x' \end{pmatrix}_{before} \quad (1)$$

The first matrix represents the linear focusing transport about the ring and is determined by the transverse tunes (ν_x,ν_y) and "betatron" functions β_x,β_y. We choose $\beta_x = \beta_y = \beta_0 = 2$ m, simulating $\bar{p}p$ collisions.

The second matrix is the non-linear beam-beam interaction caused by passage through the electromagnetic field of the opposite beam bunch in a collision region. The opposite bunch is approximated by a round "gaussian" shaped beam of RMS size σ which is unchanged from turn to turn so that:

$$F = \frac{1-e^{\frac{-(x^2+y^2)}{2\sigma^2}}}{(x^2+y^2)/2\sigma^2} \quad (2)$$

$\Delta\nu$, the "beam-beam tune shift", determines the strength of the interaction, and we choose σ = .0816 mm to duplicate $\bar{p}p$ collider values.[15] The simulation procedure approximates conditions in a $\bar{p}p$ collider: "zero-length" - "weak-strong" 2-D collisions of round beams without "synchrotron radiation". Collisions are "weak-strong" since the opposite "strong" beam is unchanged from turn to turn as in the collisions of a lower density $\bar{p}$ bunch with protons, and "zero-length" in that collisions are approximated by a simple velocity change (Bunches are short compared to the storage ring circumference.).

Tune modulation is an important process in $\bar{p}p$ colliders and is simulated by changing the tunes from turn to turn following:

$$\nu_x = \nu_{xo} + a_x \sin\left(\frac{2\pi}{N_x} n\right)$$
$$\nu_y = \nu_{yo} + a_y \sin\left(\frac{2\pi}{N_y} n\right) \qquad (3)$$

where a_x, a_y are the modulation amplitudes, N_x, N_y are the modulation periods and n is the turn number. In our modulation simulations we choose $a_x = \pm a_y$ and vary $N_o = N_x = N_y$. We note that $N_o \cong 1000$ is near the expected modulation frequencies of "power supply ripple" and "uncorrected chromaticity". a_x, a_y are chosen $\lesssim \Delta\nu = .01$ in agreement with expected collider magnitudes.

In a typical simulation initial positions for a set of 100 trajectories are chosen randomly from a 4-D gaussian phase space distribution determined by β_o and σ and tracked through many thousands or millions of turns. Individual trajectories are inspected for significant changes, as well as RMS amplitudes for the particle set, the x and y "emittances":

$$\varepsilon_x \equiv 6\sqrt{\langle x^2\rangle \langle x'^2\rangle} \qquad (4)$$

and their RMS sums: $$\varepsilon_R \equiv 6\sqrt{\varepsilon_x^2 + \varepsilon_y^2} \quad .$$

In previous publications and internal reports we have reported results of these simulations for a variety of cases corresponding to different simulation conditions. In the next two sections we summarize some features of these results related to the following theoretical model.

1B Chaotic Motion and the "2-D" Beam-Beam Interaction

Our simulations have determined that large numbers of "chaotic" trajectories can occur in simulations of the 2-D beam-beam interaction [5,9,11] under certain conditions described below. We have used a "reversability" test as an empirical tool in separating "chaotic" from "non-chaotic" motion. In this test an individual particle trajectory is tracked forward in time for

many turns. The motion is then reversed by reversing the velocity and the matrices determining the motion. Forward and return positions are compared.

Figure 1 shows results of reversability tests for sample trajectories (ν_x = .245, ν_y = .12, $\Delta\nu$ = .01) with 60 million turns forward and return (120 million turns total). Initial and final positions agree to 14 decimal places in a double precision test (10^{-28} error in one turn). Similar results are obtained in our simulation for all "normal" non-chaotic trajectories, and this indicates the amount of normal accumulated error in our simulations.

Reversability tests of some other trajectories show substantially different behavior, and a typical case is shown in Figure 2. These trajectories, which we label "chaotic", develop errors of order 1 in a few tens of thousands of turns in an exponential manner.

In "normal" trajectories, errors δ grow as simple powers of the number of turns N

$$\delta \cong \delta_o N^{\alpha}$$

where δ_o is a single turn error size (10^{-28}) and $\alpha \lesssim 2$ in our simulations. "Chaotic" trajectory errors grow exponentially

$$\delta \cong \delta_o e^{aN}$$

where a is identifiable with the "Lyapunov exponent" of the trajectory and depends on the details of the transformation. In a typical beam-beam case described below $a = O(10^{-3})$.

We have reported results of a systematic search for chaotic motion in 2-D simulations [9,11] as functions of ν_x, ν_y, $\Delta\nu$ and now summarize these results. We find that chaotic motion occurs when the "tune spread" $\Delta\nu$

contains the intersection of low order resonances. A resonance is determined by a relationship between the tunes

$$m\nu_x + n\nu_y = p$$

where m, n and p are integers and our symmetry requires that m and n be even (or zero). The order Ω of the resonance is $\Omega = |m| + |n|$.

The dependence of chaotic motion on resonance order is shown in Figure 3. In each case the resonance intersection is placed in the center of the tune spread and 100 trajectories are tested for chaotic motion by a reversability test. The results are:

1. Intersections of 4th and 6th order resonances show large regions of chaotic motion (10-30%).

2. Intersections of 4th or 6th order with 8th order also show some chaotic motion ($\lesssim$ 5%).

3. Higher order intersections show little or no chaotic motion ($\lesssim$ 1%).

4. Cases with $\nu_x = \nu_y$ (or $\nu_x = \nu_y \pm .5$) show no chaotic motion. These cases have a kinematic invariant ($p_\theta = xy'-yx'$ in these cases) which, with the energy invariant, makes the motion integrable. This reduces the motion to 1-D with diminished "chaotic" behavior.[16]

Dependence on $\Delta\nu$ has also been explored by varying $\Delta\nu$ from .005 to .02. The density of chaotic motion shows no dependence on $\Delta\nu$; however the mean Lyapunov exponent $\bar{a}$ is directly proportional to $\delta\nu$.

The 2-D motion shows no RMS amplitude instability even in a very long time scale simulation (120 million turns)[3,4]. This indicates that the appearance of chaotic motion need not lead to RMS amplitude instability.

1C Results of Simulations with Tune Modulation

We have also completed several studies of the beam-beam interaction with tune modulation and now summarize some results of these simulations. We have found that tune modulation can lead to large numbers of chaotic trajectories and to "beam blow-up" if the modulation[7,13] carries the beam across low order resonances. Figure 4 shows the modulation in a case (ν_x = .3439, ν_y = .1772, $\Delta\nu$ = .01, $a_x = -a_y$ = .005) which carries the beam across sixth order resonances. At N = 1000, ~50% of the orbits are chaotic and a fast beam blow-up occurs with a mean growth time of ~25,000 turns.

This case has been studied in greater detail by varying the modulation period N from 8 up to 100,000 [10,13]. Some of the results are displayed in Figure 5. We see no chaotic motion for $N \lesssim 32$. For $32 \lesssim N \lesssim 200$ a few chaotic trajectories appear without beam blow-up. For $N \gtrsim 200$ chaotic motion accompanied by "fast" beam blow-up occurs.

As $N \to \infty$, the existence of chaotic motion with RMS emittance growth appears to persist. The fraction of phase space containing chaotic motion remains approximately constant but the Lyapunov exponents and the RMS emittance growth rates decrease as $N \to \infty$.

2. Resonances and Resonance Overlap: Comparison of Theoretical Model Results and Simulations

In the following sections we describe calculations of resonance locations and widths in the 2-D beam-beam interaction. A resonance overlap criterion is used to estimate the area of "chaotic" motion, and the Lyapunov exponents are compared with resonance oscillation frequencies.

The resonance model is extended to include tune modulation and a modulation subresonance overlap criterion for modulational "blow-up". The characteristics of this blow-up are compared with the features of the theoretical model. Useful predictions for future colliders are obtainable.

2A The Beam-Beam Hamiltonian and the Action Angle Formalism

The matrix multiplications of Equation (1) are equivalent to integration of the following equations of motion:

$$x'' + k_x(s)x = \frac{-4\pi\Delta\nu}{\beta_o} \frac{\left(1-e^{-r^2/2\sigma^2}\right)}{(r^2/2\sigma^2)} x\ \delta_p(s)$$

$$y'' + k_y(s)y = \frac{-4\pi\Delta\nu}{\beta_o} \frac{\left(1-e^{-r^2/2\sigma^2}\right)}{(r^2/2\sigma^2)} y\ \delta_p(s) \qquad (5)$$

where β_o, $\Delta\nu$ are the interaction region C-S betatron amplitudes [17] and beam-beam tune shift, $r^2 = x^2+y^2$, $\delta_p(s)$ is a periodic delta function representing the short distance beam-beam crossing, and $k_x(s)$, $k_y(s)$ are periodic focusing functions representing the storage ring. s, the distance traveled along the ring, is the independent variable. The beam-beam interaction is that due to a "strong" beam with a gaussian density:

$$\rho(r) = \rho_o\, e^{-r^2/2\sigma^2} = \frac{N_{tot}}{2\pi\sigma^2}\, e^{-r^2/\sigma^2}\ . \qquad (6)$$

The nonlinear beam-beam force can be rewritten as the gradient of a potential function

$$x'' + k_x(s)x = \frac{-4\pi\Delta\nu\ \sigma^2}{\beta_o} \frac{\partial}{\partial x} U(x,y)\ \delta_p(s)$$

where

$$U = \int_o^{r^2/2\sigma^2} \frac{1-e^{-t}}{t}\, dt \qquad (7)$$

$$= E_{in}\left(\frac{r^2}{2\sigma^2}\right)$$

where $E_{in}(u)$ is the "exponential integral function" (see Abramowitz and Stegun [18], p. 228). It has the power series representation

$$E_{in}(u) = \sum_{1}^{\infty} \frac{(-1)^{n-1} u^n}{n!n} . \tag{8}$$

For large u, this approaches

$$E_{in}(u) \cong .5772 + \log(u)$$

where log is the natural logarithm.

The Hamiltonian corresponding to these equations of motion is:

$$H = \frac{1}{2}(p_x^2 + k_x(s)x^2) + \frac{1}{2}(p_y^2 + k_y(s)y^2)$$

$$+ \frac{4\pi\Delta\nu}{\beta_o} \sigma^2 U(x,y) \delta p(s). \tag{9}$$

The Hamiltonian can be transformed into action-angle coordinates by the generating function

$$G(x,y,\phi_x,\phi_y) = -\frac{x^2}{2\beta_x}\left[\tan\phi_x - \frac{\beta_x'(s)}{2}\right]$$

$$-\frac{y^2}{2\beta_y}\left[\tan\phi_y - \frac{\beta_y'(s)}{2}\right]$$

$$\Phi_x = \phi_x + \int_o^s ds' \left(\frac{1}{\beta_x(s')} - \frac{\nu_x}{R}\right) \tag{10}$$

where Φ_y is given by the same equation as Φ_x with the exchange of x for y.

After the canonical transformation and a change of independent variable from s to $\theta = s/R$, we find

$$H = \nu_x I_x + \nu_y I_y$$

$$+ \delta_p(\theta) A\, U(x,y) \tag{11}$$

with

$$A = \frac{4\pi\Delta\nu}{\beta_o}\sigma^2 \quad \text{and} \quad x = \sqrt{2I_x\beta_o}\cos\phi_x$$

(note that with round beams $\beta_x = \beta_y = \beta_o$).

Expansion in Fourier series obtains:

$$U\delta_p(\theta) = \frac{1}{2\pi}\sum_{m,n,p} f_{mn}(I_x,I_y)e^{i(m\phi_x+n\phi_y-p\theta)} \tag{12}$$

where

$$f_{mn}(I_x,I_y) = \frac{1}{(2\pi)^2}\int_0^{2\pi}\int_0^{2\pi} d\phi_x\, d\phi_y\, e^{-i(m\phi_x+n\phi_y)} \cdot$$

$$\cdot E_{in}\left(\frac{\beta_o I_x\cos^2\phi_x + \beta_o I_y\cos^2\phi_y}{\sigma^2}\right) . \tag{13}$$

Our new Hamiltonian is

$$H(I,\phi,\theta) = \nu_x I_x + \nu_y I_y$$

$$+ A\sum \frac{f_{mn}}{2\pi}(I_x,I_y)\, e^{i(m\phi_x+n\phi_y-p\theta)} . \tag{14}$$

The average "tune" as a function of I_x, I_y can be obtained by ignoring the time varying part of (14):

$$\bar{\nu}_x = \frac{\partial H}{\partial I_x} = \nu_x + \frac{A}{2\pi}\frac{\partial f_{oo}}{\partial I_x}$$

$$= \nu_x + \delta\nu\; g_x\left(\frac{I_x}{I_o}, \frac{I_y}{I_o}\right) \qquad \left(I_o = \frac{\sigma^2}{\beta_o}\right) \tag{15}$$

g_x is a function of the amplitudes with values between 0 and 1 and is displayed graphically in Figure 6. Note that:

$$g_x \cong g_y \text{ for most } I_x, I_y$$

also:

$$g_x \to 1 \text{ as } I_x \text{ and } I_y \to 0$$

$$g_x \to 0 \text{ as } I_x \text{ or } I_y \to \infty.$$

2B The Hamiltonian in the Resonance Approximation

A resonance is obtained where

$$m\bar{\nu}_x + n\bar{\nu}_y = p \tag{16}$$

with m, n, p integers. In the resonance approximation we keep only the lowest order resonant terms of H.

$$H = \nu_x I_x + \nu_y I_y + \frac{A}{2\pi} f_{oo} + \frac{A f_{mn}}{\pi} \cos(m\phi_x + n\phi_y - p\theta). \tag{17}$$

The time variable can be removed from (17) by transforming to new variables

$$\psi_x = \phi_x - \nu_{xo}\theta$$

where ν_{xo}, ν_{yo} are resonant tunes within the tune spread with

$$m\nu_{xo} + n\nu_{yo} = p$$

$$H = (\nu_x-\nu_{xo})I_x + (\nu_y-\nu_{yo})I_y$$

$$+ \frac{A}{2\pi} f_{oo} + \frac{A}{\pi} f_{mn} \cos(m\psi_x+n\psi_y). \tag{18}$$

This can be transformed into resonance coordinates by

$$I^+ = \frac{mI_x+nI_y}{\sqrt{n^2+m^2}}$$

$$I^- = \frac{nI_x-mI_x}{\sqrt{n^2+m^2}} \tag{19}$$

$$\psi^+ = \frac{m\psi_x+n\psi_y}{\sqrt{n^2+m^2}}$$

$$\psi^- = \frac{n\psi_x-m\psi_y}{\sqrt{n^2+m^2}} \quad .$$

The new Hamiltonian is:

$$\bar{H} = \frac{1}{\sqrt{n^2+m^2}}\left(m(\nu_x-\nu_{xo}) + n(\nu_y-\nu_{yo})\right)I^+$$

$$+ \frac{1}{\sqrt{n^2+m^2}}\left(n(\nu_x-\nu_{xo}) - m(\nu_y-\nu_{yo})\right)I^- \tag{20}$$

$$+ \frac{Af_{oo}}{2\pi} + \frac{Af_{mn}}{\pi} \cos(\sqrt{n^2+m^2}\ \psi^+).$$

This is independent of ψ^-, so I^- is a constant of the motion. Resonant amplitudes I_x, I_y or I_o^+, I_o^- are found from

$$\left[\frac{1}{\sqrt{n^2+m^2}}\Big(m(\nu_x-\nu_{xo}) + n(\nu_y-\nu_{yo})\Big) + \frac{A}{2\pi}\frac{\partial f_{oo}}{\partial I^+}\right] = 0 \tag{21}$$

which can be satisfied by

$$-(\nu_x-\nu_{xo}) = \frac{A}{2\pi}\frac{\partial f_{oo}}{\partial I_x} \text{ and } -(\nu_y-\nu_{yo}) = \frac{A}{2\pi}\frac{\partial f_{oo}}{\partial I_y}. \tag{22}$$

A resonance width can be obtained around this reference point from

$$\bar{H} \cong \frac{A}{4\pi}\frac{\partial^2 f_{oo}}{\partial I^{+2}}(I^+-I_o^+)^2 + \frac{Af_{nm}}{\pi}\cos(\sqrt{n^2+m^2}\,\psi^+) + \text{constant} \tag{23}$$

which is recognizable as the Hamiltonian of a pendulum. The resonance width (full width) is

$$\Delta I^+ = 2\sqrt{\frac{8f_{nm}}{f_{oo}''}} \tag{24}$$

where

$$f_{oo}'' = \frac{\partial^2 f_{oo}}{\partial I^{+2}}.$$

Resonance width decreases with increasing resonance order ($|m|+|n|$) and also depends on the amplitudes $(I_x)_o$, $(I_y)_o$ at which it is evaluated. For sample cases let us choose $I_{xo} = I_{yo}$ such that $g_x = g_y = \frac{1}{2}$

so that the resonances lie precisely in the center of the tune spread. We find, numerically, that this occurs at $I_x = I_y \cong 1.35\ I_o$. In Table I we tabulate calculated values of the resonance integrals and widths for this case for even n,m; $|n|+|m| \leq 8$. (These integrals are zero if n or m is odd.)

2C Resonance Overlap and Chaotic Motion

In References [5,9] we discovered that chaotic motion occurs at the intersection of two independent resonances. The Hamiltonian at another resonance

$$j\nu_{xo} + k\nu_{yo} = p$$

is the same as Equation (20) with new resonance variables (J^+, J^-). If we choose ν_{xo}, ν_{yo} at the intersection of the two resonances, we find

$$H \cong \frac{A}{4\pi}\left[\frac{\partial^2 f_{oo}}{\partial I_x^2}\Delta_x^2 + \frac{2\partial^2 f_{oo}}{\partial I_x \partial I_y}\Delta_x\Delta_y + \frac{\partial^2 f_{oo}}{\partial I_y^2}\Delta_y^2\right]$$

$$+ \frac{A}{\pi}\left[f_{nm}\cos(\sqrt{n^2+m^2}\ \psi^+_{nm}) + f_{jk}\cos(\sqrt{j^2+k^2}\ \psi^+_{jk})\right] \qquad (25)$$

$$+ \text{constant}$$

which is reduced to a coupled pendulums Hamiltonian about the resonance amplitudes I_{xo}, I_{yo}; which are chosen at the intersection of two resonances.

In Reference [5] "chaotic" motion was observed near the intersection of low order resonances in this "resonance overlap" region. In this note we observe that the size of this chaotic region can be estimated by calculating this overlapping area in I_x, I_y space:

$$\text{Chaotic Area} = \Delta I^+ \cdot \Delta J^+ \cdot |\cos(u_{ij})| \qquad (26)$$

where

$$|\cos u_{ij}| = \frac{|mk-nj|}{\sqrt{m^2+n^2}\sqrt{j^2+k^2}}$$

depends on the relative orientation of the resonances in I_x, I_y space ($\cos u_{ij} = 1$ if the resonances are orthogonal.), and ΔI^+, ΔJ^+ are the full widths of the two resonances.

The probability that a randomly selected trajectory is chaotic can be estimated by the expression

$$P(\text{chaotic}) \cong f(I_{xo}, I_{yo})\ \Delta I^+\ \Delta J^+\ |\cos U_{ij}| \tag{27}$$

where $f(I_{xo}, I_{yo})$ is the central probability density.

In Reference [9] the probability of chaotic motion is measured for various cases of resonance intersections in simulation. For these cases $I_{xo} = I_{yo} = 1.35\ I_o$ and

$$f(I_x, I_y) = \frac{1}{I_o^2}\ e^{-\frac{(I_x+I_y)}{I_o}} . \tag{28}$$

In Table 2 we compare the simulation results in which chaotic motion in randomly selected trajectories is observed with the above "probability of chaotic motion" for various resonance intersections. Qualitative and quantitative agreement is good, indicating that the above estimation method is fairly accurate.

The results show all distinguishable crossings of fourth and sixth order resonances, eliminating cases with $\nu_x = \nu_y$. (In the cases with $\nu_x = \nu_y$ an invariant of the motion $p_\theta = x'y-y'x$ exists which reduces the motion to 1-D; no 2-D resonance intersections of the type analyzed here can exist.)

Eighth order resonances have widths $\sim\frac{1}{3}$ that of sixth order ones at our parameters, and therefore should show $\sim\frac{1}{3}$ as much chaotic motion in intersections with fourth or sixth order resonances as corresponding 6th order intersections. Simulation results show ~1-5% chaotic motion in agreement with the theoretical model.

Higher order resonances have still smaller widths and should produce very little chaotic motion, in agreement with simulations.

The results are in fact fortuitously close. In the model we have ignored higher order resonances, which would increase the chaotic region, and regions of nonchaotic motion within the resonance overlap ("islands of stability"). The errors have fortuitously cancelled.

2D Small Oscillation Frequency and Lyapunov Exponents

An important parameter in chaotic motion is the rate of divergence of adjacent trajectories. This is given by the Lyapunov exponent in a relationship such as

$$\delta \cong \delta_0 \, e^{at}$$

where δ is the size of the distance between trajectories, δ_0 is an initial value and a is the Lyapunov exponent.

In chaotic motion of coupled pendulums, a is expected to be of the same magnitude as the pendulum oscillation frequencies. In a beam-beam resonance the equations of motion are

$$\frac{d\psi^+}{d\theta} = \frac{A}{2\pi} f''_{oo} \, \Delta I^+ \tag{29}$$

$$\frac{d\Delta I^+}{d\theta} = + \frac{A}{\pi} f_{nm} \sqrt{n^2+m^2} \cdot \sin\left(\sqrt{n^2+m^2}\, \psi^+\right)$$

which gives us a small oscillation ω_{so} frequency near fixed points (where $\dot{I}^+ = \psi^+ = 0$) of

$$\omega_{so} = \sqrt{\frac{A^2}{2\pi^2}(n^2+m^2)f_o'' f_{nm}} \tag{30}$$

ω_{so} is also tabulated in Table 1 for the low order resonances.

For the chaotic trajectories of case B of Reference [1] ($\nu_x = .245$, $\nu_y = .12$, $\Delta\nu = .01$) the mean Lyapunov exponent was

$$\bar{a} \cong .00037$$

in the present units. The intersecting low order resonances have $\omega_{so} = .0034$, .002 and .0012. $\bar{a}$ is of the same magnitude but somewhat lower as would be expected from a more complete analysis of the coupled oscillations.

In Reference [9] we showed that $\bar{a} \propto \Delta\nu$ in simulations. This is expected since $\omega_{so} \propto \Delta\nu$ in Equation (30). In the same simulations the probability of chaotic motion was <u>independent</u> of $\Delta\nu$. This is in agreement with our resonance overlap model since resonance <u>widths</u> in the beam-beam interaction are independent of $\Delta\nu$.

2E Tune Modulation and the Beam-Beam Interaction

The Hamiltonian can be modified to include tune modulation by the substitution (see Equation (4))

$$\nu_i \to \nu_i + \Delta_i \cos(\nu_s \theta + \phi_i) \tag{31}$$

where ν_s is the modulation frequency, Δ_x is the modulation amplitude and ϕ_i is the phase. To simplify discussion we choose $\phi_x = \phi_y = 0$ and $\nu_{sx} = \nu_{sy} = \nu_s$. The single resonance Hamiltonian (Equation 18) becomes

$$\begin{aligned} H = {} & (\nu_x - \nu_{xo} + \Delta_x \cos \omega_s\theta)I_x \\ & + (\nu_y - \nu_{yo} + \Delta_y \cos \omega_s\theta)I_y \\ & + \frac{Af_{oo}}{2\pi} + \frac{A}{\pi} f_{mn} \cos(m\psi_x + n\psi_y). \end{aligned} \tag{32}$$

After transforming to the resonance coordinates I^+, ψ^+ we obtain

$$H = \frac{I^+}{\sqrt{m^2+n^2}} \left[\delta\nu_{mn} + \Delta \cos(\nu_s\theta) \right] + \frac{Af_{oo}}{2\pi} + \frac{A}{\pi} f_{mn} \cos(\sqrt{n^2+m^2}\ \psi^+) \tag{33}$$

where $\Delta = m\Delta_x + n\Delta_y$ and $\delta\nu_{mn} \equiv m(\nu_x-\nu_{xo}) + n(\nu_y-\nu_{yo})$ and we have removed I^-, ψ^- from the Hamiltonian as nonresonant. We choose a new variable

$$\phi^+ = \psi^+ - \frac{\Delta \sin(\nu_s\theta)}{\nu_s\sqrt{n^2+m^2}}$$

which removes the time varying term from the first term of Equation (33) and changes the cosine argument to

$$\cos\left(\sqrt{n^2+m^2}\ \phi^+ + \frac{\Delta}{\nu_s} \sin \nu_s\theta\right) = \sum_{k=-\infty}^{\infty} J_k\left(\frac{\Delta}{\nu_s}\right) \cos(\sqrt{n^2+m^2}\ \phi^+ + k\nu_s\theta). \tag{34}$$

We have exchanged our single resonance Hamiltonian for one containing an infinite number of subresonances (see Courant [19] for a similar treatment of a different case):

$$H = \frac{I^+}{\sqrt{m^2+n^2}} \delta\nu_{mn} + \frac{Af_{oo}}{2\pi} + \frac{Af_{mn}}{\pi} \sum_k J_k\left(\frac{\Delta}{\nu_s}\right) \cos(\sqrt{n^2+m^2}\ \phi^+ + k\nu_s\theta). \tag{35}$$

In each such subresonance this can be rewritten as:

$$H_k \cong \frac{I^+}{\sqrt{m^2+n^2}} (\delta\nu_{mn} + k\nu_s) \tag{36}$$

$$+ \frac{Af_{oo}}{2\pi} + \frac{Af_{mn}}{\pi} J_k(\frac{\Delta}{\nu_s}) \cos(\sqrt{n^2+m^2}\ \psi_k^+).$$

The subresonances are spaced $\nu_s/\sqrt{m^2+n^2}$ apart in tune, with their central amplitudes, found from the solution of

$$\frac{(\delta\nu_{mn} + k\nu_s)}{\sqrt{m^2+n^2}} + \frac{Af'_{oo}}{2\pi} = 0 \tag{37}$$

spaced in amplitude by

$$\delta I_+ = \frac{2\pi\nu_s}{Af''_{oo}\sqrt{m^2+n^2}} . \tag{38}$$

If the resonance width is greater than the resonance spacing then the "Chirikov" overlap criterion is satisfied[14], and we may expect "stochastic motion" and particle trajectories which travel from resonance to resonance.

This "overlap criterion" is

$$2\sqrt{\frac{8f_{nm}\ J_k(\frac{\Delta}{\nu_s})}{f''_{oo}}} \gtrsim \frac{2\pi\nu_s}{Af''_o\sqrt{m^2+n^2}} \tag{39}$$

or (with $A = 4\pi\Delta\nu$)

$$\nu_s \lesssim 8\Delta\nu\sqrt{f_{nm}\ f''_o(n^2+m^2)J_k(\frac{\Delta}{\nu_s})2} . \tag{40}$$

Absolute values are taken in all expressions.

In Reference[10] simulations of the beam-beam interaction with tune modulation were reported in which ν_s was varied while the other parameters (ν_x, ν_y, $\Delta\nu$, Δ_x) were fixed at values (.3439, .1772, .01, .005) which swept the beam across sixth order resonances. It was found that no chaotic motion occurs for modulation period $N \equiv 1/\nu_s \gtrsim 32$ turns. For $32 \lesssim N \lesssim 100$ a few chaotic trajectories appear while for $N \gtrsim 200$ ($\nu_s \lesssim .005$) large numbers of chaotic trajectories appear and "beam blow-up" (RMS amplitude increase) occurs.

We can estimate the threshold in ν_s for this case using parameters obtained from Table (1) in Equation (40). With $\Delta = .01$, $f_{nm} \cong .0027$, $f_o'' = .065$, $n^2+m^2 = 2^2+4^2 = 20$, and noting that for Δ/ν_s small, $J_k(\Delta/\nu_s)$ is maximum for $k = 0$ with a value of ~1, we obtain $\nu_s = .0067$ ($N = 150$) as the threshold modulation frequency for resonance overlap, which is in reasonable agreement with the beam blow-up threshold observed in simulations.

Another simulation result is that there is no lower limit in ν_s for stochastic beam blow-up; as $N \to \infty$ the same fraction of trajectories are chaotic although the rate of beam blow-up and magnitude of Lyapunov exponents decreases. This result can be explained in terms of the resonance overlap criterion, noting first that

$$J_k\left(\frac{\Delta}{\nu_s}\right) \sim \sqrt{\frac{2\nu_s}{\pi\Delta}} \quad \text{as } \nu_s \to 0.$$

Thus subresonance width ($\propto \nu_s^{\frac{1}{4}}$) and subresonance spacing ($\propto \nu_s$) both decrease as $\nu_s \to 0$. However since the spacing decreases more rapidly the overlap criterion (width > spacing) remains satisfied as $\nu_s \to 0 (N \to \infty)$.

3. Discussion and Comparison

From the simulations and the discussion above, we have determined that chaotic motion occurs in the overlap region of intersecting 2-D resonances

and that chaotic motion with beam blow-up occurs in simulations with tune modulation in which modulation subresonances intersect. No beam blow-up is seen in the unmodulated 2-D cases. In these cases the overlapping resonances are centered on the same amplitudes so stochastic motion of trajectories between the resonances does not lead to RMS amplitude increase. However, with tune modulation the subresonances are centered at different amplitudes and stochastic motion of particles between subresonances can lead to RMS amplitude changes and "beam blow-up". The analysis of the motion in terms of resonance overlap is thus able to explain qualitatively this phenomenon.

The results presented in this paper have shown that a simplified resonance model with analysis of resonance overlap is capable of qualitative and quantitative estimation of conditions for chaotic motion and "beam blow-up" in simulations of the beam-beam interaction. We note here that Evans and Gareyte [20] have seen evidence for beam blow-up due to tune modulation in $\bar{p}p$ collisions. The above analysis and simulations [1-13] are useful in understanding the observations and extending the results to further collider cases.

Acknowledgements

We are grateful to Alessandro Ruggiero for his support and participation in the beam-beam project and for his assistance in the analysis. We are also grateful to Alan Riddiford for his competent programming assistance in the simulations.

References

1. D. Neuffer, A. Riddiford and A. Ruggiero, IEEE Trans. NS-28, p. 2494 (1981)
2. D. Neuffer and A. Ruggiero, FN-325, Proc. of the Beam-Beam Interaction Seminar, SLAC-Pub-2624, p. 332 (1980)
3. D. Neuffer, A. Riddiford and A. Ruggiero, Fermilab Note FN-333 (1981)
4. D. Neuffer et al., FN-343 (1981)
5. D. Neuffer et al., FN-346 (1981)
6. D. Neuffer et al., Fermilab Memo TM-1007 (1980)
7. D. Neuffer et al., FN-357 (1981)
8. D. Neuffer et al., FN-358 (1982)
9. D. Neuffer et al., FN-363 (1982)
10. D. Neuffer et al., FN-373 (1982)
11. D. Neuffer, A. Riddiford and A.G. Ruggiero, Proc. of the 1983 Particle Accelerator Conference, to be published in IEEE Trans. NS-30 (1983)
12. D. Neuffer, A. Riddiford and A.G. Ruggiero, to be published in IEEE Trans. NS-30 (1983)
13. D. Neuffer, A. Riddiford and A.G. Ruggiero, to be published in IEEE Trans. NS-30 (1983)
14. B.V. Chirikov, Physics Reports 52C, p. 265 (1979)
15. Tevatron I Design Report, Fermilab, February 1982
16. A.G. Ruggiero, Particle Accelerators 12, p. 45 (1982)
17. E.D. Courant and H.S. Snyder, Ann. of Phys. 3, 1 (1958)
18. M. Abramowitz and A. Stegun, Handbook of Mathematical Functions, U.S. Government Printing Office, Washington, D.C. (1964)
19. E.D. Courant, ISABELLE Tech. Note 163, Brookhaven National Laboratory (1980)
20. L. Evans and J. Gareyte, CERN SPS/82-8 (1982)

Table 1 Resonance parameters at $I_{xo} = I_{yo} = 1.35\ I_o$, $\Delta\nu = .01$

Resonance			$\lvert f_{nm}\rvert$	$I_o^2\lvert f''_{oo}\rvert$	ΔI^+	ω_{so}
m	n					
2	0	4th order	.027	.103	2.88	.0042
4	0		.014	.065	2.60	.0034
4	2	6th order	.0027	.096	0.95	.0020
4	-2		.0027	.034	1.59	.0012
6	0		.00091	.065	0.34	.0013
4	4	8th order	.00036	.103	0.33	.00097
4	-4		.00036	.027	0.66	.00050
6	2		.00024	.079	0.31	.00078
6	-2		.00024	.051	0.39	.00063
8	0		.000064	.065	0.18	.00046
6	4	10th order	.000021	.100	0.082	.00030
10	0		.0000015	.065	0.027	.00009

Table 2 Chaotic Motion at Resonance Intersection

Tunes ν_x, ν_y	Resonances ($\leq$ 6th order)	% Chaotic Motion (Theory)	% Chaotic Motion (Simulation)
.333, .167	$2\nu_x+2\nu_y = 1$	35	30
	$4\nu_x-2\nu_y = 1$		
	$2\nu_x-4\nu_y = 0$		
	$6\nu_x = 2$		
	$6\nu_y = 1$		
.250, .125	$4\nu_x = 1$	18.8	21
	$4\nu_y+2\nu_x = 1$		
	$4\nu_y-2\nu_x = 0$		
.30, .10	$4\nu_y+2\nu_x = 1$	10.1	12
	$4\nu_x-2\nu_y = 1$		
.25, .167	$4\nu_x = 1$	11.9	11
	$6\nu_y = 1$		
.167, .125	$6\nu_x = 1$	6.4	6
	$4\nu_y-2\nu_x = 0$		

Figure Captions

Figure 1: Results of reversability tests for three non-chaotic trajectories

Figure 2: Results of a reversability test for a chaotic trajectory

Figure 3: Number of chaotic trajectories from 100 randomly selected initial conditions as functions of ν_x, ν_y at $\Delta\nu = 0.01$. In each case the resonance intersection is in the center of the tune spread.

Figure 4: Tune modulation at $\nu_x = .3439$, $\nu_y = .1772$, $\Delta\nu = .01$, $a_x = -a_y = .005$. Low order resonances swept by the tune spread are indicated.

Figure 5: Chaotic motion and beam emittance growth as a function of tune modulation period N at the tune parameters of Figure 4

Figure 6: Mean x and y tune shifts $\Delta\nu_x$, $\Delta\nu_y$ as function of particle amplitudes I_x, I_y. ($\Delta\nu_x(I_x,I_y)$, $\Delta\nu_y(I_x,I_y)$ obey the symmetry relation $\Delta\nu_x(I_1,I_2) = \Delta\nu_y(I_2,I_1)$.)

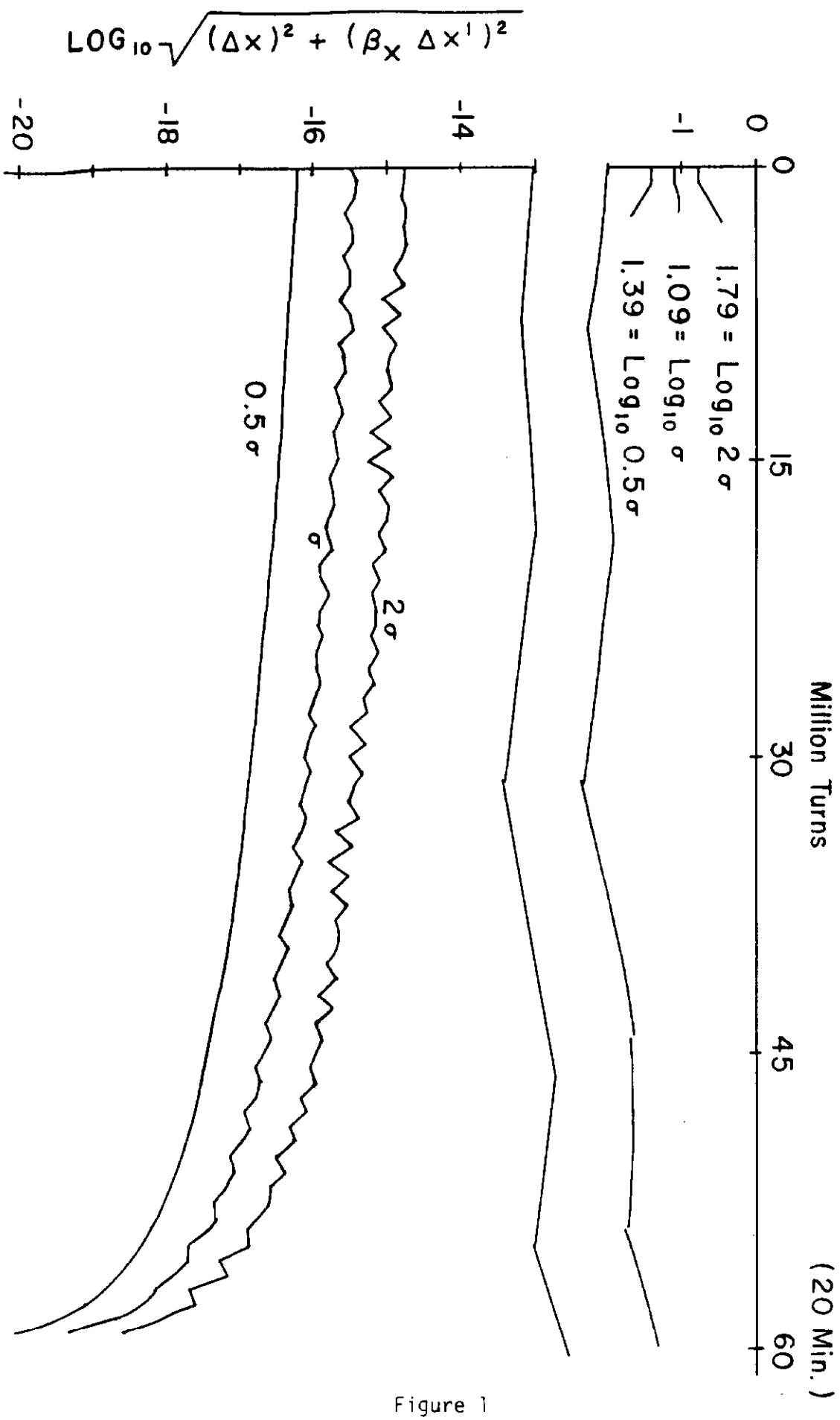
$LOG_{10}\sqrt{(\Delta x)^2 + (\beta_x \Delta x')^2}$
-20
-18
-16
-14
0.5 σ
σ
2σ
0
-1
1.79 = Log10 2 σ
1.09 = Log10 σ
1.39 = Log10 0.5σ
0
15
30
45
60
Million Turns
(20 Min.)

Figure 1

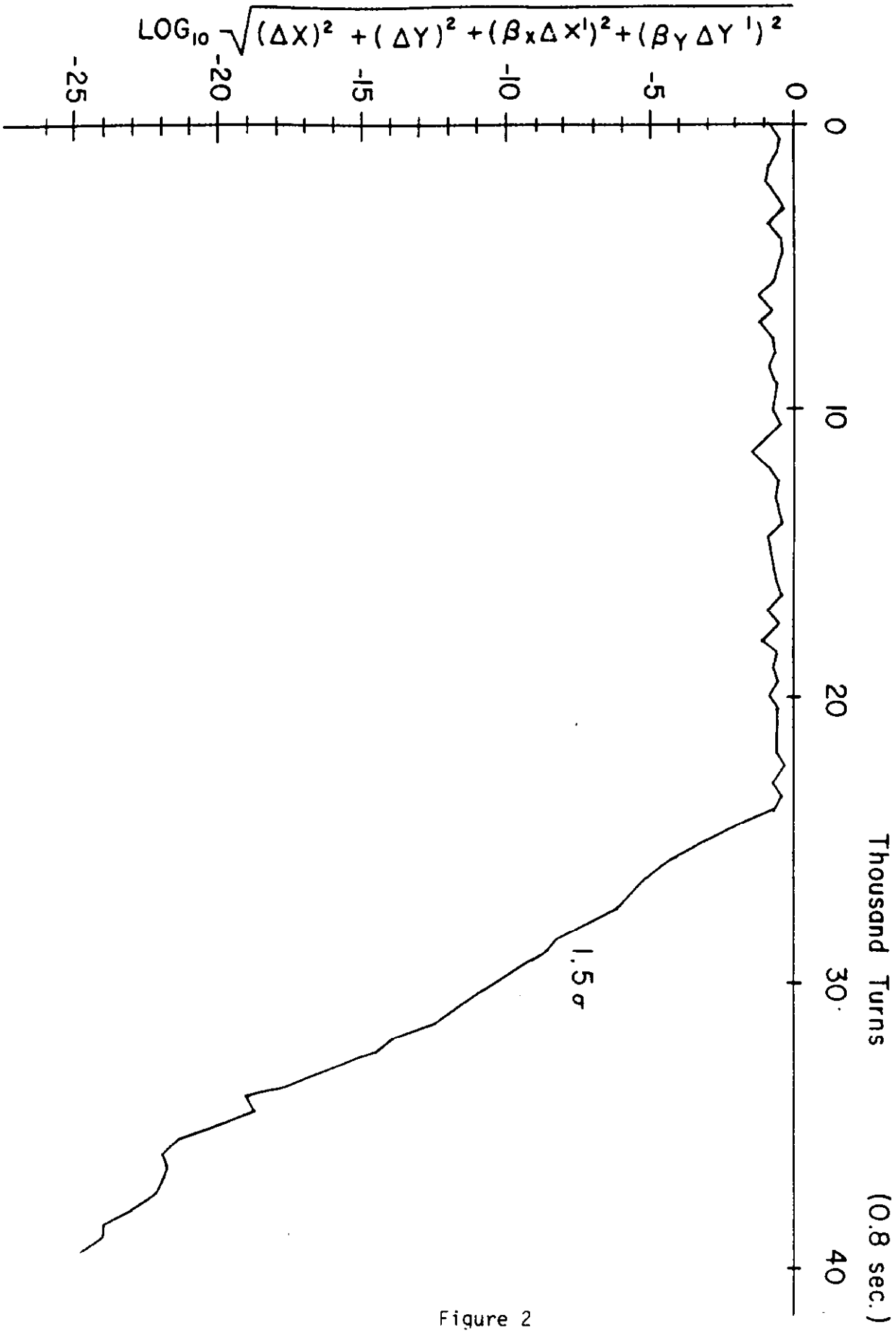
$LOG_{10}\sqrt{(\Delta X)^2 + (\Delta Y)^2 + (\beta_x \Delta X')^2 + (\beta_Y \Delta Y')^2}$
-25
-20
-15
-10
-5
0
0
10
20
30
40
Thousand Turns
(0.8 sec.)
1.5 σ

Figure 2

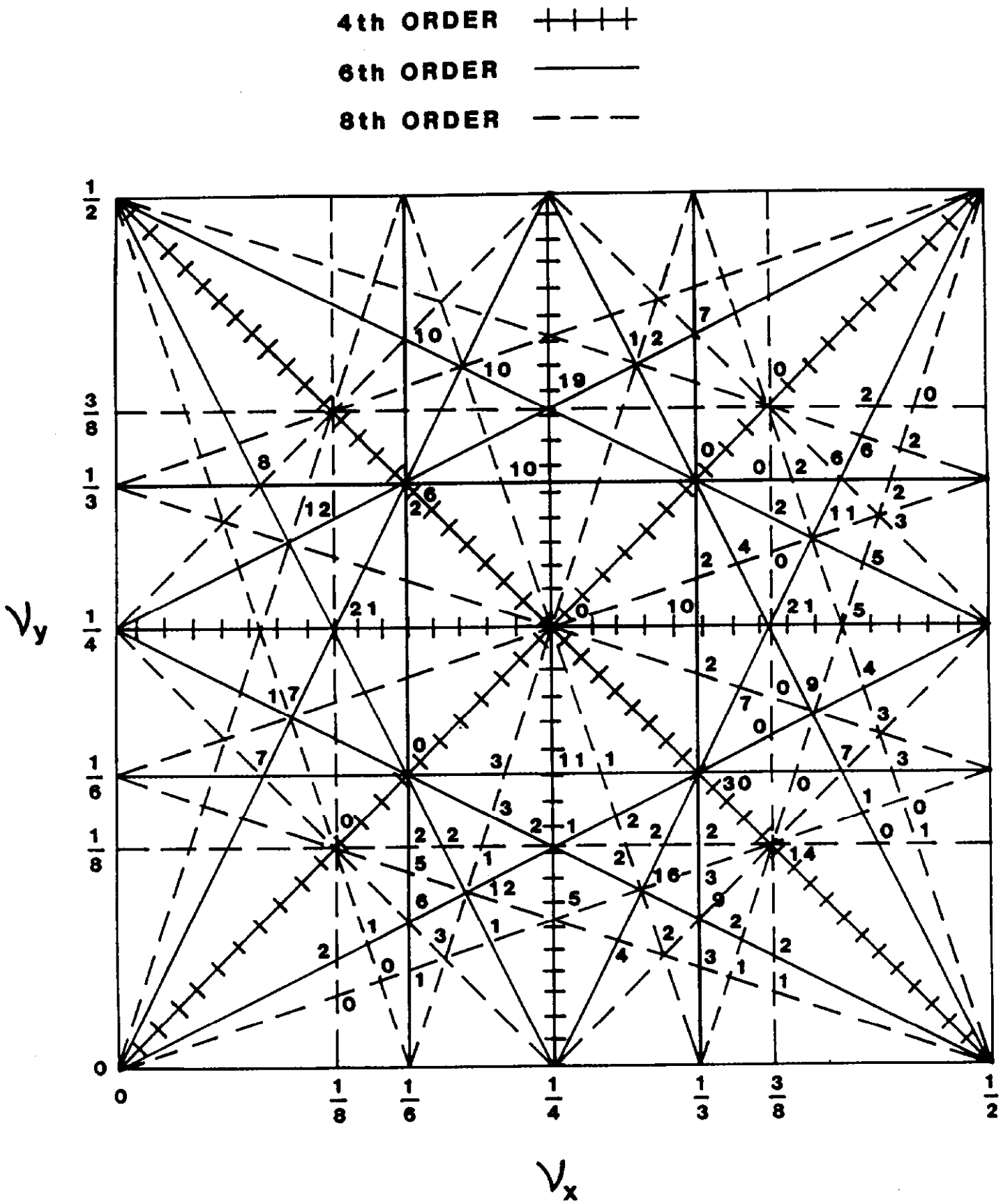
4th ORDER
6th ORDER
8th ORDER
ν_y
ν_x
0
$\frac{1}{8}$
$\frac{1}{6}$
$\frac{1}{4}$
$\frac{1}{3}$
$\frac{3}{8}$
$\frac{1}{2}$

Figure 3

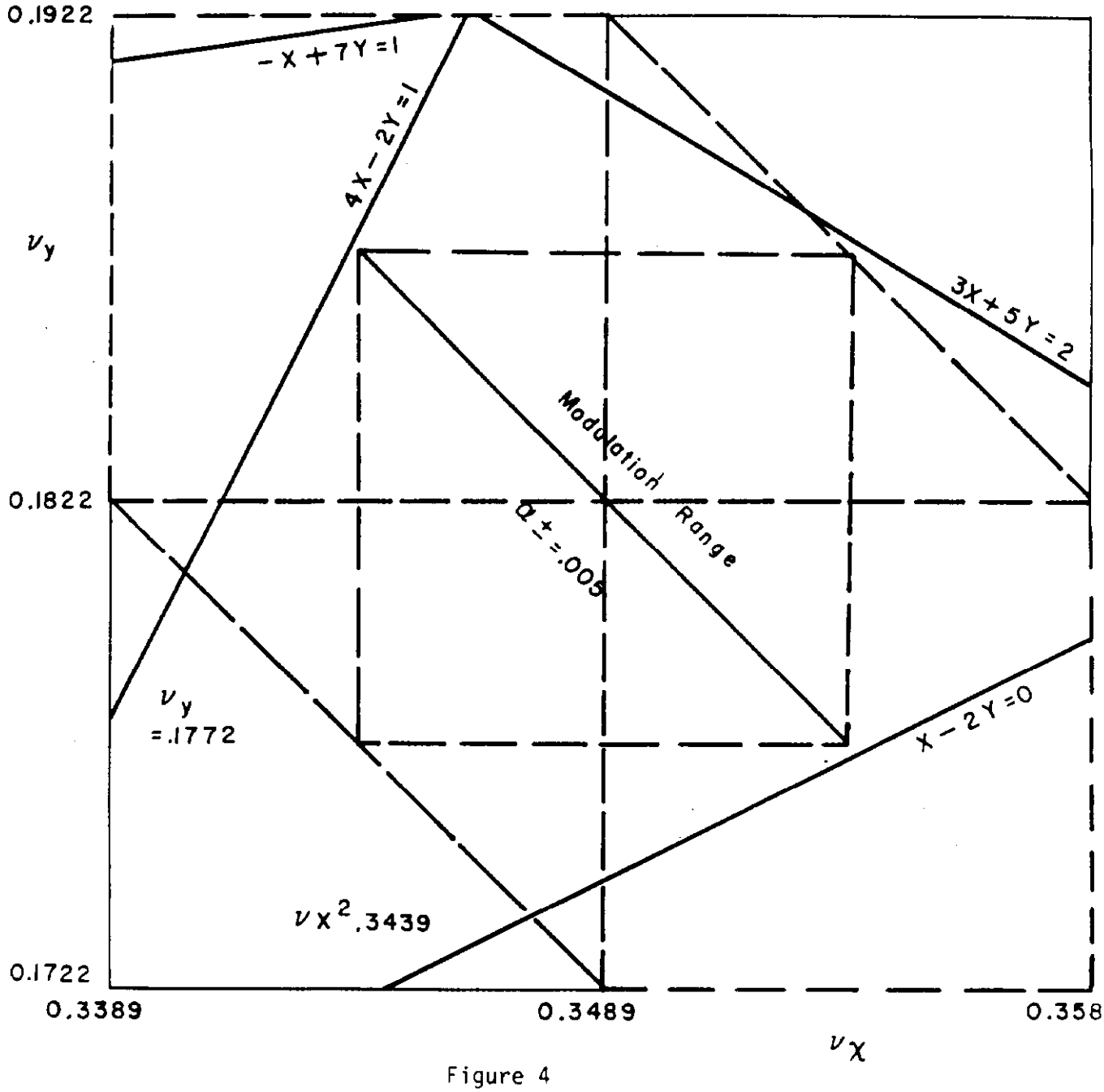
0.1922
0.1822
0.1722
ν_y
$-X+7Y=1$
$4X-2Y=1$
$3X+5Y=2$
Modulation
Range
$\alpha_{\pm}=.005$
ν_y
$=.1772$
$X-2Y=0$
$\nu x^2 .3439$
0.3389
0.3489
0.358
ν_x

Figure 4

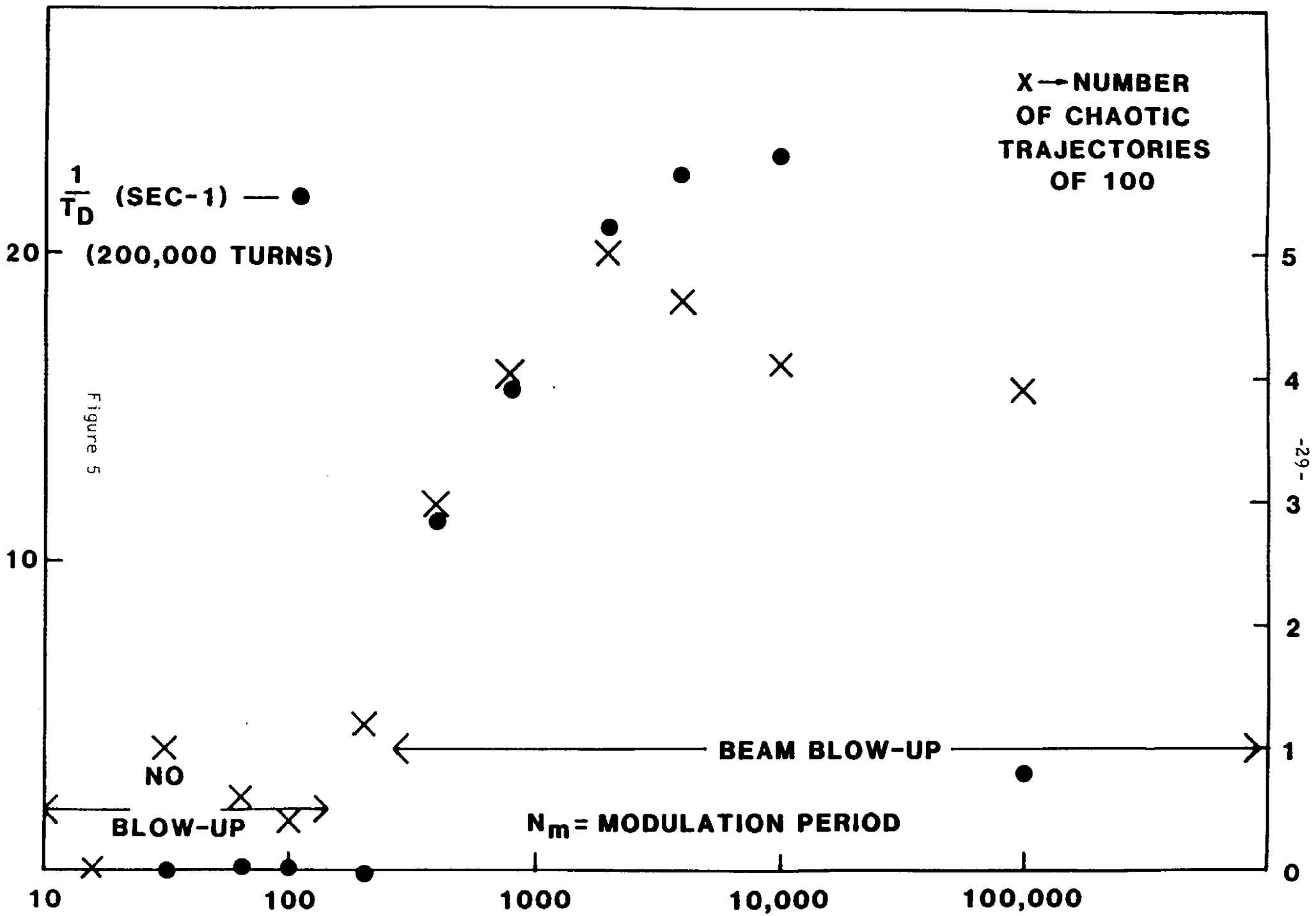
X → NUMBER OF CHAOTIC TRAJECTORIES OF 100
$\frac{1}{T_D}$ (SEC-1) —
(200,000 TURNS)
20
10
5
4
3
2
1
0
NO BLOW-UP
BEAM BLOW-UP
N_m = MODULATION PERIOD
10
100
1000
10,000
100,000

Figure 5

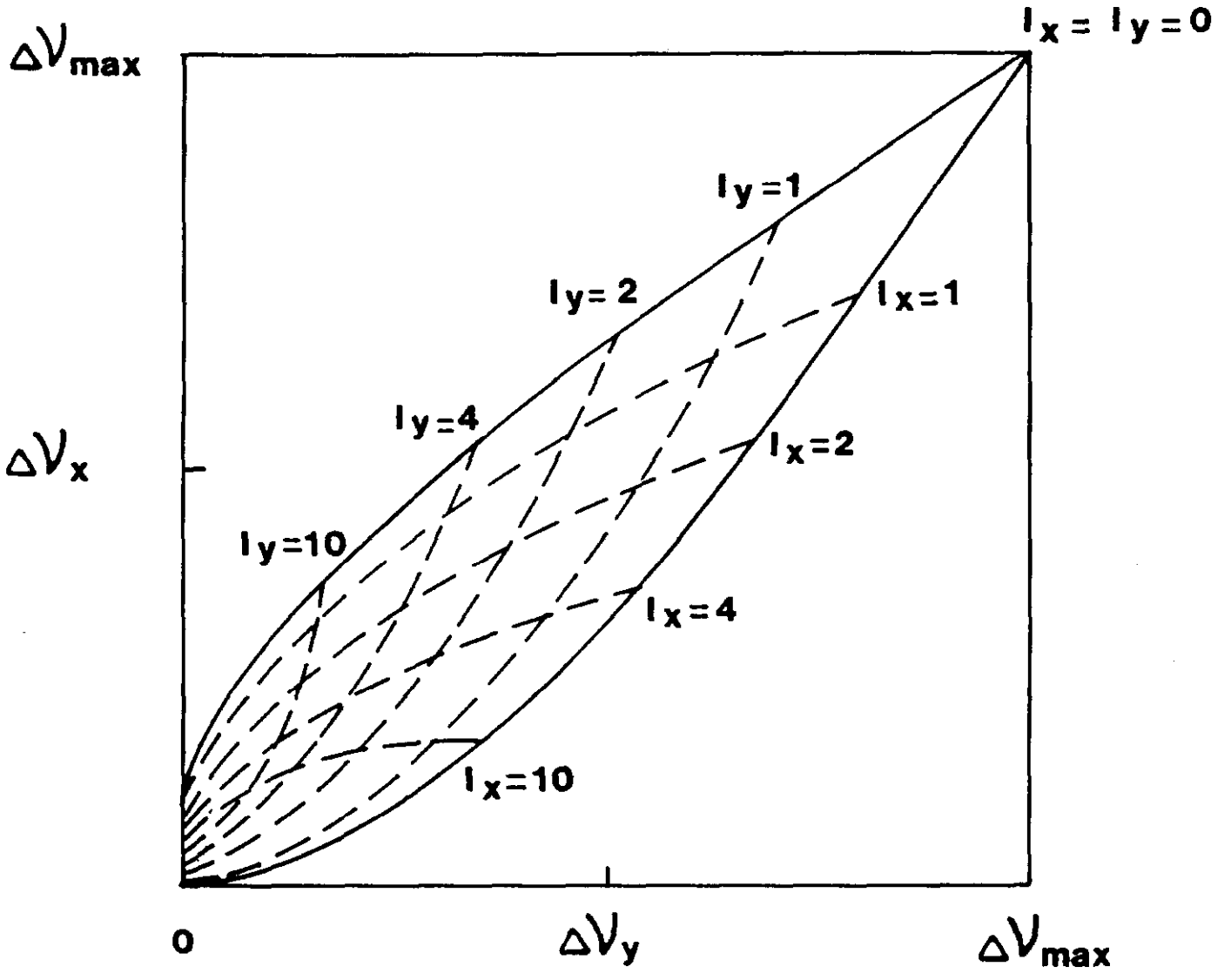
ΔV_{max}
$I_x = I_y = 0$
$I_y = 1$
$I_y = 2$
$I_x = 1$
$I_y = 4$
$I_x = 2$
ΔV_x
$I_y = 10$
$I_x = 4$
$I_x = 10$
0
ΔV_y
ΔV_{max}

Figure 6